Manipulating emission of CdSe/ZnS nanocrystals embedded in 3D photonic crystals

Céline Vion, Carlos Barthou, Paul Bénalloul, Catherine Schwob, Laurent Coolen, Alex Gruzintev, Gennadi Emelchenko, Wladimir Masalov, Jean-Marc Frigerio, Agnès Maître

Manipulating emission of CdSe/ZnS nanocrystals embedded in 3D photonic crystals

Céline Vion[1],* Carlos Barthou[1], Paul Bénalloul[1], Catherine Schwob[1], Laurent Coolen[1], Alex Gruzintev[2], Gennadii Emel'chenko[3], Vladimir Masalov[3], Jean-Marc Frigerio[1], and Agnès Maître[1]

(1) Institut des NanoSciences de Paris, UMR-CNRS 7588, Université Pierre et Marie Curie, F-75015 Paris, France

(2) Institut of Microelectronics Technology and High Purity Materials, Russian Academy of Science, 142432, Chernogolovka, Moscow District, Russia and

(3) Institute of Solid State Physics, Russian Academy of Science, 142432, Chernogolovka, Moscow District, Russia

(Dated: November 18, 2008)

Abstract

We report experimental and theoretical results on the photoluminescence of CdSe/ZnS core-shell nanocrystals, embedded in a silica opaline structure by infiltration of a highly diluted solution. Strong modification of emission diagrams of embedded nanocrystals have been observed in good agreement with theoretical models. At macroscopic scale, we measured the difference of lifetime between an opal infiltrated with nanocrystals with emission wavelength in the pseudogap and an opal with smaller balls size for which the nanocrystal emission wavelength is outside the pseudogap. The photonic bandgap effect leads to an increase of the lifetime of the order of 4%. These lifetime variations are shown to be in good agreement with the calculated local density of states modification due to the pseudogap.

PACS numbers: 42.50.Nn; 42.70.Qs, 61.72.uj; 61.46.Hk; 78.67.Bf

*Electronic address: celine.vion@insp.jussieu.fr

I. INTRODUCTION

Photonic crystals are characterized by a periodic dielectric constant at wavelength scale, creating photonic energy bands where light propagation is forbidden. The emission of light sources embedded inside a photonic crystal can be strongly affected by these bandgaps: according to Fermi's golden rule, the rate of spontaneous emission is proportional to the photonic local density of states (LDOS), which describes the interaction between emitters and the local field in the sample. As the photonic local density of states is strongly dependant on the material structure, photonic crystals are used for tailoring the emission of embedded light sources. This active field of research leads to applications ranging from quantum information processing [1], to light emitting devices (miniature lasers) [2] or solar cells [3].

Most devices use 2-dimensions (2D) photonic crystals, consisting in a lattice of holes etched in a high index transparent material. In the weak coupling regime, emission of single quantum dots in 2D photonic crystals has been improved, as well for their photoluminescence intensity [4] as for the polarization of emission [5]. In the strong coupling regime [6], achieved with InAs quantum dots embedded in a GaAs photonic crystal membrane, vacuum Rabi splitting [7] and emission of indistinguishable single photons [1] have been demonstrated. All these devices have been realized by electron lithography, requiring heavy technological equipments. Alternatively to this top-down approach, impregnation of 2D photonic crystals with solutions of colloïdal nanocrystals is a versatile way to couple emitters to photonic structures and to allow enhancement of spontaneous emission [8, 9].

Moreover, spontaneous self-organization of spherical colloidal particles is an attractive alternative to produce photonic crystals. Indeed, various techniques provide a low-cost and relatively easy protocol to obtain synthetic opals. It has been shown that the quality of opaline structures strongly depends on synthesis techniques [10]. Just as in 2D photonic crystals, the spontaneous emission of optical sources embedded in direct and inverted opals is affected by the crystal structure and can be inferred by the local density of states [11]. However, the modification of spontaneous emission lifetime by 3D silica opals is reported to be weak since the refractive index contrast is low (below 5% for an index contrast of 1.2) [12]. Larger effects require a higher refractive contrast and a complete photonic band gap which can be obtained in inverted opals [13–15]. For colloidal CdSe nanocrystals

infiltrated in titania inverse opals, lifetime reductions up to 30% have been reported [16]. Nevertheless, good quality inverse opals over large scale are still difficult to synthesize and most experimental studies on coupling emitters to 3D photonic crystals have been achieved in opals exhibiting a pseudo-band gap (infiltrated with nanocrystals [17–22] or molecules [14, 23–25]).

Even incomplete, the photonic bandgap affects both the luminescence spectrum of the emitter and its spontaneous lifetime. Nevertheless, disorder in opal structures can hide or limit these phenomena. To get rid of the disorder, experiments have to be performed at a scale smaller than the typical size of the opal for which it can be considered as a monocrystal. The use of a microscope can reveal the quality of the opals at a micronic scale by selection of a high quality opal zone [17, 25]. At this scale, stop-band effect on nanocrystals luminescence spectra [26], single nanocrystal emission modification [17] and sligth effects on luminescence lifetime [25] have been reported. Nevertheless the pseudo gap effect is averaged over the whole numerical aperture of the microscope objective, and the dip in fluorescence spectrum due to the gap disappears for a large aperture [23]. Therefore, the use of a microscope limits the possibilities to study angle-resolved luminescent properties and does not reveal the quality of the opal over a large scale (mm) which is essential for applications.

The aim of this work is to study at macroscopic scale the coupling of colloidal core/shell CdSe/ZnS nanocrystals to artificial direct opals. In the first part, we present the preparation and optical characterization of opaline structures. The second section presents the modification of nanocrystals emission diagrams. In a third section, a lifetime modification due the photonic bandgap is evidenced and interpreted by LDOS calculations.

II. OPALS CHARACTERIZATION

The opals were prepared by sedimentation of 270 nm diameter silica balls in suspension in water, with a post selection of the 0.5 mm thick upper part of the deposit. The balls got organized spontaneously as a face-centered-cubic (fcc) structure according to the highest density plane (111). The samples were then dried at 150°C, and annealed at 600°C during 5 hours in free atmosphere. Robust 5x5x0.5 mm^3 samples were obtained ($\approx$ 2300 layers) [27,

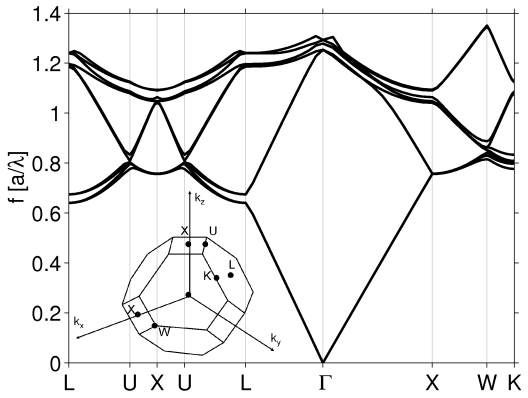

FIG. 1: Photonic band structure of the fcc lattice calculated with effective index n_{eff}=1.34 as a function of reduced frequency $f = a/\lambda$ (where a is the primitive cell parameter $a = \sqrt{2}D$, with D the diameter of the balls), for wave vectors between the high symmetry points X, U, L, Γ, K and W of the Brillouin zone.

28]. Fig. 1 presents the opal band diagram calculated numerically by a direct computation of the eigenstates and eigenvalues of Maxwell's equations (using a planewave basis) [29], showing a photonic pseudogap at the L point of the photonic Brillouin zone.

The opals were optically characterized by specular reflection, from which the diameter of the balls and the effective refracting index of the medium were inferred. The sample was illuminated with a fiberred and collimated halogen source covering the whole 350-800nm spectral range, and the reflected ligth was collected by a second optical fiber symmetric to the first one. The fibers were mounted on rotating stages allowing a precise selection of the incident and collection angles. The light spot on the opal had a size of 4mm^2(at 20° incidence) and the distance between the sample and the optical fiber was 10 cm.

As the first bandgap of the direct opal is not complete, light propagation in this frequency range is allowed for certain directions and prohibited for others. Indeed, an important reflectivity is awaited for the wavelengths for which the phase difference induced by reflexions on two consecutive (111) planes of the face-centered cubic lattice is a multiple of 2π. This condition is fulfilled for an incidence angle corresponding to the Bragg angle which can be expressed as [30]:

$$\lambda_{max} = 2\sqrt{(2/3)}D\sqrt{(n_{eff}^2 - \sin^2(\phi))} \quad (1)$$

where D is the diameter of the balls, ϕ is the incidence angle relative to the normal of the (111) plane and n_{eff} is the effective refractive index of the medium with n_{eff} =

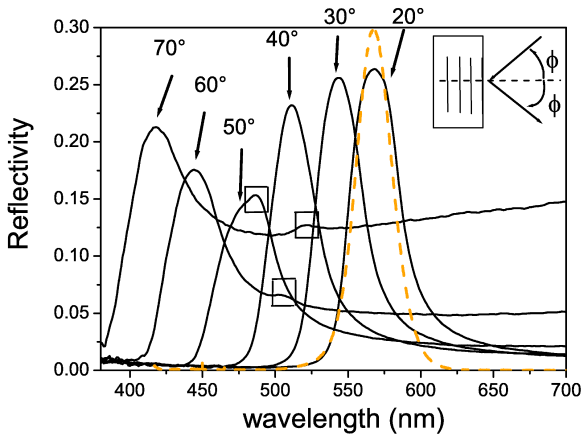

(a)

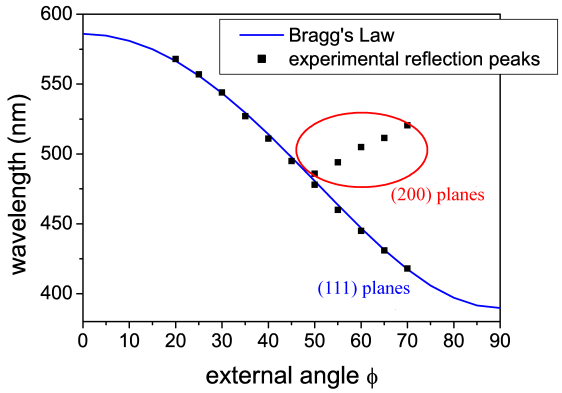

(b)

FIG. 2: (a) Reflectivity spectrum of an opal for various incidence angles. (squares indicate the position of the second peaks) Dashed line: nanocrystals luminescence spectrum, (b) Comparison of the experimental results with Bragg's law (Eq.1): D=269nm, n_{eff}=1.34

$\sqrt{\alpha\epsilon_{silica} + (1-\alpha)\epsilon_0}$, and α is the filling factor ($\alpha = 0.74$ for close packed structures).

Fig. 2a presents the spectra obtained by specular reflexion on the opal for non polarized light at different incidence angles. The reflectivity is approximately 20% for frequencies inside the gap in spite of the large illuminated spot size which demonstrates a good quality of the samples over a large scale for the (111) planes. The wavelengths for which the specular reflectivity is maximum are plotted according to the angle of incidence. An adjustment with Bragg's law (Fig. 2b) yields with a precision of 5% the diameter of the balls $D = 269$ nm and the effective index of the structure $n_{eff} = 1.34$ corresponding to an index of the silica $n_{silica} = 1.44$. This diameter is in good agreement with the measurements performed with an atomic force microscope.

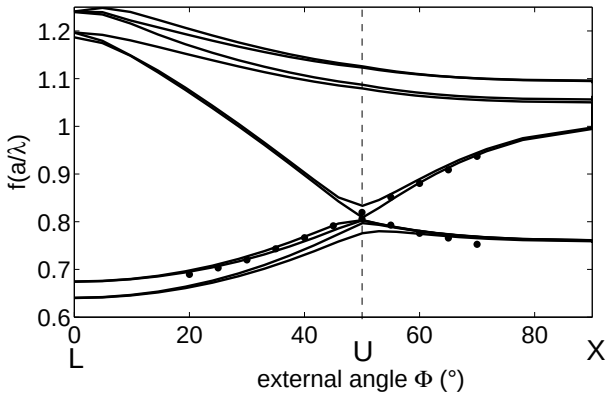

FIG. 3: Photonic band structure (solid line) calculated along the LU and UX line expressed as a function of incidence angle for 269nm balls size opal. The circles indicate the experimental peaks associated with (111) and (200) planes.

At an angle ϕ larger than 50°, a second peak appears on the reflection spectra (see Fig. 2.a). This peak unlike the first one shifts towards higher wavelengths for increased incident angles, as described in PMMA-sphere opals [32]. The interpretation of this phenomenon requires exact band structure calculations. On Fig. 3 the photonic band structure calculated along the LU and UX lines inside the first Brillouin zone (for $n_{eff} = 1.34$) is superimposed on the experimental peaks of specular reflection spectra as a function of the external incidence angle ϕ, which is related by Snell's law $\sin(\phi) = n_{eff}\sin(\theta)$ to the internal angle θ with the L direction normal to the (111) plane. At the U point (corresponding to an external angle ϕ of 50.2°), a second pseudo-gap can be attributed to the constructive interference reflections on the planes (200). The observation of this second peak, implying coherent reflections on other planes than the (111) ones, demonstrates the good face-cubic-centered crystallinity of the opal.

III. MODIFICATION OF NANOCRYSTALS EMISSION DIAGRAMS

We focus first on emission diagram modifications of nanocrystals embedded in the opal. We use a nanomolar solution of CdSe/ZnS nanocrystals (Qdot Invitrogen 565 ITK) diluted in decane of index $n_{decane} = 1.41$, a value close to the measured silica index ($n_{balls} = 1.44$). The luminescence spectrum of the solution is centered at 565 nm and presents a Full Width Half Maximum (FWHM) of 30 nm. The previously studied opal is infiltrated with $1\mu L$

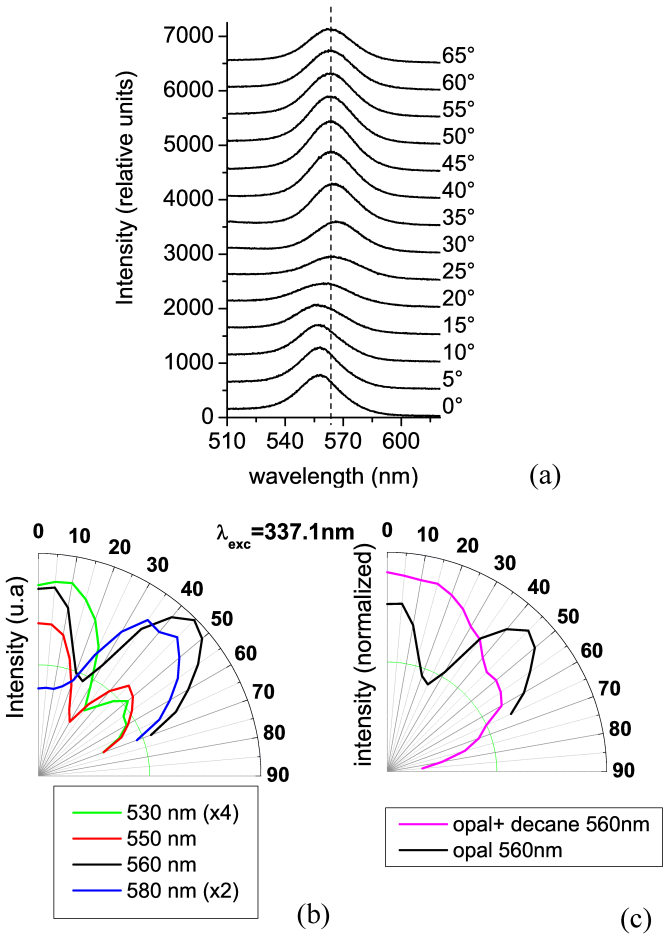

FIG. 4: (a)Luminescence spectra of infiltrated nanocrystals in an 269nm balls size opal sample at different collection angles (the spectra are shifted for clarity). (b)Diagrams of radiation of infiltrated nanocrystals at different wavelengths. (c)Diagrams of radiation at 560 nm of nanocrystals in opal (black line) compared to nanocrystals in opal infiltrated with decane (purple line).

of this solution and becomes translucent, demonstrating that the solution spread all over the opal: the decane infiltrated opal is close to an homogeneous medium with an effective index of 1.43. As a consequence, the nanocrystals are distributed randomly in the whole volume of the sample, with much less than one nanocrystal per void. Indeed, this low density of emitters prevents nanocrystals agregation and interactions among them, and the optical properties of the opal are not modified : after 15 min, the decane solution is totally evaporated, and specular reflection spectra realized on the infiltrated opal are identical to the ones realized prior to infiltration.

The infiltrated nanocrystals are then excited at a wavelength of 337.1 nm by a pulsed nitrogen laser (0.6 ns pulse width). Their luminescence is collected by an optical fiber mounted on a rotary stage and located at a distance of 10 cm from the surface. In this setup, for an illumination spot of $1mm^2$ size on the opal surface, the detection angle resolution is approximately 1°. The emission is analyzed with a spectrometer coupled to a nitrogen-cooled Si Charged-Coupled Device (CCD) detector. This setup has a wavelength resolution of 0.3 nm/point. The experimental specular spectra are plotted in Fig. 4a for different collection angles. As the FWHM of quantum dots luminescence spectrum is of the same order as the stop band FWMH, the incidence angle dependant gap does not induce a dip on luminescence spectra but induces a narrowing of the linewidth of the nanocrystal emission and a shift of the peak wavelength (see Fig. 4a). Depending of the angle of collection, the central wavelength of the emission line is shifted from 556nm to 566nm and the linewidth is reduced from 30 to 25 nm. In Fig. 4b, the radiation diagrams are plotted as a function of the angle of detection ϕ for different wavelengths. For each wavelength, a strong reduction of luminescence is observed for specific angles. In Fig. 5, these specific wavelengths for which quantum dots luminescence is reduced, are plotted as a function of the external angle ϕ. The curve is fitted by Bragg's law, like the central wavelength photonic bandgap measured previously by specular reflexion (Fig. 2). In order to confirm the influence of the crystalline structure, the infiltrated opal is filled with a solution of decane, removing the gap. The dip in the emission diagram of nanocrystals disappears for the decane filled sample, as expected for an homogeneous medium (Fig. 4c). These results are a clear demonstration of the modification of nanocrystals spontaneous emission diagrams by the photonic bandgap.

IV. MODIFICATION OF NANOCRYSTALS EMISSION LIFETIME

Let us now consider the influence of the photonic crystal on the nanocrystals emission decay rate. We experimentally compare the lifetime of nanocrystals embedded in opals having different balls size: 242nm and 269nm. For the 242nm and 269nm balls size opal the gap is respectively located at 530nm and 615nm at 0° incidence. We performed the experiment at two different wavelengths: 565nm and 575nm by selecting spectrally with a monochromator the emission of the nanocrystals. For the 269nm balls size opal the nanocrystal emission is located in the gap and for 242nm balls size opal the nanocrystal emission is outside the gap.

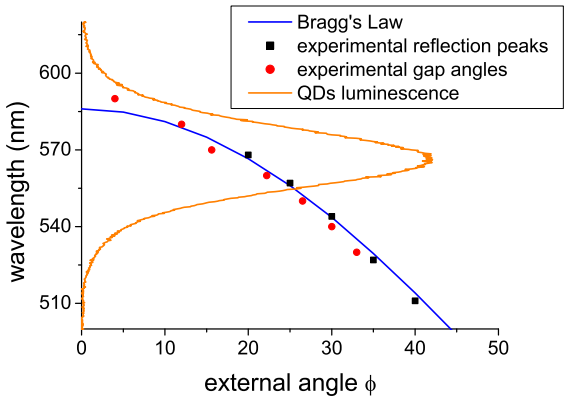

FIG. 5: Comparison of the experimental results with Bragg's law for 269nm balls size opal. Orange line: quantum dots in decane luminescence spectra. The red circles indicate the position of the minima on the diagrams of radiation. The black squares are the position of the reflection maxima.

It should be noted that by selecting to different wavelengths, we select two different populations of nanocrystals with slightly different emission properties, so that a direct comparison between the two measurements can not be achieved.

The emission wavelength is selected by the spectrometer, and the decay curves are measured by a photomultiplier coupled to an oscilloscope. The time constant of our setup is of one nanosecond. In the following, the fiber is settled orthogonal to the surface.

As seen on Fig. 6, opals exhibit self-luminescence under 337nm excitation wavelength, but this luminescence decay is much faster than the nanocrystals one. It can be seen on the emission spectrum (inset on Fig. 6) that, for such pulsed excitation, self luminescence is more than 10 times less intense than nanocrystals emission. Even if, for times shorter than 10 ns, the fast self-luminescence of silica balls influences the decay curves, after 10 ns it can be considered as negligible. The nanocrystal luminescence lifetimes are therefore calculated by fitting the decay curves for times between 10ns and 150ns. We fit the non-exponential decay curves with a continuous log-normal distribution of decay rates as suggested by the group of Vos et al [31], and used with success in references [15] and [25]. The decays are modeled with a continuous distribution of decay rates:

$$I(t) = I(0) \int_{\gamma=0}^{\infty} \Phi(\gamma) e^{-\gamma t} d\gamma \qquad (2)$$

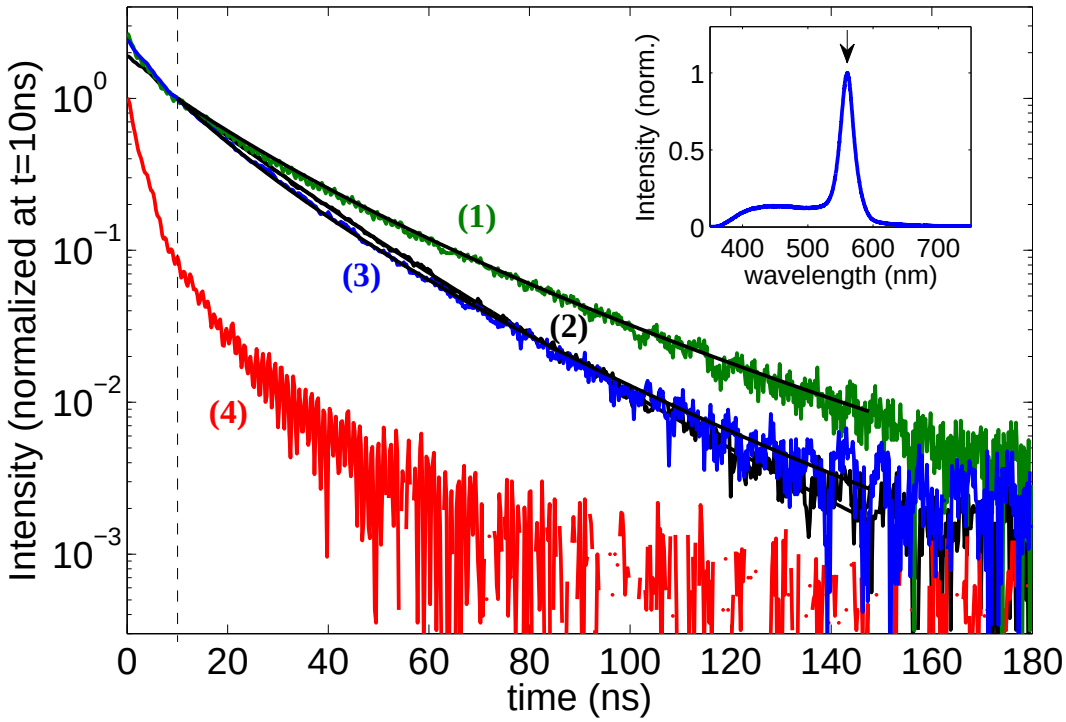

FIG. 6: Decays measured at 565nm for 269nm balls size opal. (1) Luminescence decay of nanocrystals infiltrated in the opal (green line), (2) nanocrystals in a solution of decane (black line), (3) nanocrystals in the opal infiltrated with decane (blue line). (4) Red line: self-luminescence of the opal. The fits using the log-normal distribution are plotted in black. The inset presents the luminescence spectrum at 0° collection.

with a log-normal distribution function of the form:

$$\Phi(\gamma) = A \ \exp(-\frac{\ln^2(\gamma/\gamma_{MF})}{w^2}) \tag{3}$$

where γ_{MF} is the most-frequent decay rate corresponding to the maximum of $\Phi(\gamma)$, and w is a dimensionless width parameter. The decays are fitted on more than two decades with only two free parameters γ_{MF} and w by a least squares fit with $1/y$ weighting of the data (y being the data value I(t)). The results are given in Table 1.

For both wavelengths, the spontaneous emission of the nanocrystals embedded in 269nm silica balls opal is inhibited by a factor of about 4% compared to the 242nm balls opal.

In order to explain these lifetime modifications, the variation of the local density of states at the emitter positions has been calculated. According to Fermi's golden rule, the excited

selected wavelength	opal D=242nm	opal D=269nm	difference
565 nm	$\gamma_{MF} = 0.0408ns^{-1}$	$\gamma_{MF} = 0.0390ns^{-1}$	-4.4%
	$(1/\gamma_{MF} = 24.5ns)$	$(1/\gamma_{MF} = 25.6ns)$	
	$w = 0.60$	$w = 0.62$	
575 nm	$\gamma_{MF} = 0.0392ns^{-1}$	$\gamma_{MF} = 0.0376ns^{-1}$	-4.1%
	$(1/\gamma_{MF} = 25.5ns)$	$(1/\gamma_{MF} = 26.6ns)$	
	$w = 0.60$	$w = 0.62$	

TABLE I: Most frequent decay rate (γ_{MF}) and width of the distribution (w) for opals of 242nm balls size and 269nm balls size, at 565 and 575nm detection wavelengths. The percentage of decay rate variations of 269nm balls size opal with respect to 242nm balls size opal are given in the fourth column.

state of an emitting dipole decays exponentially to the ground state with a decay constant:

$$\Gamma = \frac{2\pi}{\hbar^2} \sum_{n,\vec{k} \in BZ} | \vec{\mu} \, . \, \vec{E_{\vec{k}}} \, (\vec{r})|^2 \delta(\omega - \omega_{n,\vec{k}}) \tag{4}$$

where $\vec{\mu}$ is the dipole moment, and $\vec{E_{\vec{k}}} \, (r)$, a plane wave function, is the electric field of mode $\vec{k}$. n refers to the number of the band. The non radiative deacy chanels are neglected. The dipole moment $\vec{\mu}$ is assumed to be constant and randomly oriented in space. The decay rate expression becomes then:

$$\Gamma = \frac{2\pi}{3\hbar^2}|\mu|^2 \sum_{n,\vec{k} \in BZ} |E_{\vec{k}}(\vec{r})|^2 \delta(\omega - \omega_{n,\vec{k}}) = \frac{2\pi}{3\hbar^2}|\mu|^2 \rho(\omega, \vec{r}) \tag{5}$$

$\rho(\omega, \vec{r})$ is the photon LDOS and is strongly dependent on the index modification at wavelength scale.

Starting from the band diagrams, the distribution of electromagnetic field is calculated in the first Brillouin zone by the standard plane-wave expansion method, and the LDOS inside the opal is inferred [12]. To improve the numerical accuracy, we used a linear interpolation technique as implemented within the abinit package [33] to obtain a stable numerical result with a small number of k points in the Brillouin zone: we used 7106 k points in the first Brillouin zone (equivalent to 79507 equally spaced k points). The primitive cell was divided

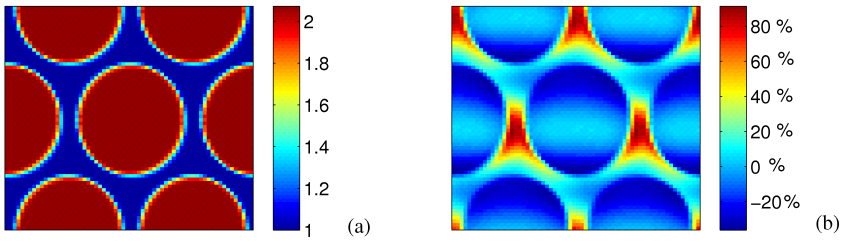

FIG. 7: (a) Assumed opal dielectric constant on a plane (111). Calculation resolution: 12 nm for 269nm balls size opal. The transition zone between silica and air has a width of 36nm (b) Calculated percentage of variation of the local density of state around its mean value in the primitive cell in the pseudo gap, at $f = a/\lambda = 0.67$ (for $a = \sqrt{2} * 269nm$ and $\lambda = 565nm$).

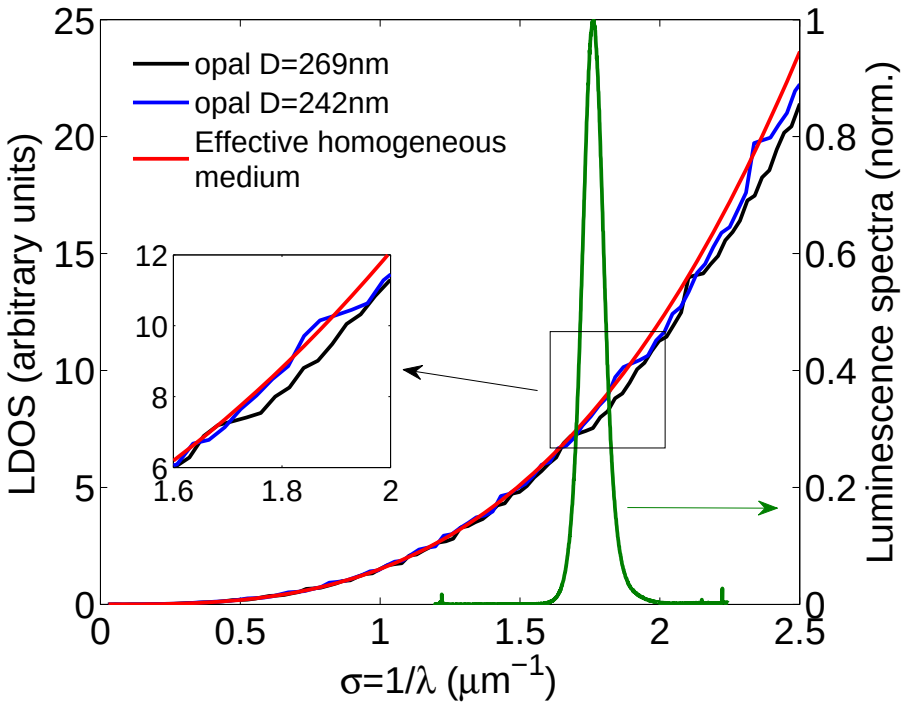

FIG. 8: Averaged LDOS at air/SiO_2 interface for opal of balls size D=269nm (black line) and D=242nm (blue line), effective homogeneous medium (red line). For the pure opal case, the LDOS is averaged on regions for which the dielectric constant varies between 1.1 and 2. Green line: luminescence spectra of nanocrystals emitting at 565nm as a function of σ.

into 32x32x32 segments, giving a resolution of 12nm. For numerical reasons, the sharp transition between the silica and air dielectric constants lead to diverging results and had to be replaced by a smoother one, of thickness equal to 3x12=36nm (see Fig. 7a).

As seen on Fig. 7b, the LDOS variation $\rho(\omega, \vec{r})$ over the cell is high and can become larger than 100% between voids and inner silica balls. As a consequence, in the simulations, the exact localization of the nanocrystals, whose diameter(core+shell) is close to 10nm, is critical. We assume that nanocrystals are randomly located in the three pixels interface between air and silica, and we calculate the average LDOS (<LDOS>= $< \rho(\omega, \vec{r}) >$) over this intermediate region for which the dielectric constant varies between 1.1 and 2.

On figure 8, we compared the variation of <LDOS> with $\sigma = 1/\lambda$ for two empty opal of respective balls sizes 269nm and 242nm, and a homogeneous medium of index $n = 1.4$. For an empty opal, two different regimes have to be discussed:

- For a reduced frequency $f = a/\lambda < 0.62$ (corresponding to $\sigma < 1.6\mu m^{-1}$ for 269nm balls size opal and $\sigma < 1.8\mu m^{-1}$ for 242nm balls size opal) the averaged LDOS can be fitted by the $< LDOS >$ of a homogeneous medium. The <LDOS> scales as ω^3 as expected for an effective homogeneous medium.

- In the band diagram of figure 1, the reduced frequency $f = a/\lambda = 0.62$ corresponds to the L point, for which the dispersion curve becomes different from the homogeneous medium, and the first photonic gap appears. For reduced frequencies larger than 0.62, the opal cannot be modeled by a homogenous medium and both the band diagram and the LDOS are modified by the crystalline structure of the opal. For $\sigma = 1.6\mu m^{-1}$ the $< LDOS >$ of the 269nm balls size opal exhibits a relative variation of 5% in comparison with the LDOS of the homogeneous medium of index 1.4. This difference increases to 10% for $\sigma = 2.5\mu m^{-1}$. The same theoretical 5% effect of the pseudogap for low index contrast opals has been reported in litterature [12, 25].

The detection wavelength 565nm corresponds to $\sigma = 1.76\mu m^{-1}$ and 575nm to $\sigma = 1.74\mu m^{-1}$. For 242nm balls size opal, the L point is moved to $\sigma = 1.8\mu m^{-1}$, so that for both wavelengths this opal is equivalent to an effective homogeneous medium and can be taken as reference. On the contrary, for 269nm balls size opal the two wavelengths are such that $\sigma > 1.6\mu m^{-1}$, the nanocrystals emission is then affected by the gap. The experimental increase of lifetime of 4% at 565nm and 575nm detection wavelengths in the 269nm balls size

opal by comparison to 242nm balls size opal is in good agreement with the LDOS calculation results. It can be then attributed to the pseudo bandgap effect.

As seen on Fig. 4, infiltrating an opal with decane successfully removed the pseudo band gap as no dip in the emission diagram of embedded nanocrystals was observed. Then, the next question will be if an opal infiltrated with decane could be interestingly used as reference to account for a bandgap effect. We compared our decay curves in opals with the decay curves in a decane solution and in decane-infiltrated opals (Fig. 6). The decay rates measured in the decane-infiltrated opals were similar to the ones measured in decane, showing that the decane-infiltrated opal is very close to an homogeneous medium. This is in agreement with our LDOS calculations (not shown here). The good reproducibility of the infiltration and evaporation steps and the coherence with the measurements in decane solution indicate that the nanocrystals are not degraded in this process.

However, between the opals and the decane infiltrated opals, we measured around 25 % increase of decay rate, which is much larger than the LDOS predictions. By taking into account effect of the pseudogap and effective homogeneous index modification, the LDOS predicts a 5% variation for the 242nm balls size opal and 10% variation for the 269nm balls size opal by comparison with the empty opal case. This experiment shows that photonic bandgap effects are not the only effects modifying the decay rate. The same conclusion was given in reference [12] to explain larger variations of lifetime compared with LDOS predictions for molecules embedded in colloidal photonic crystals. As well, for single nanocrystals on glass coverslips, large decay rate fluctuations have been reported and attributed to the opening of non-radiative decay channels due to defects at the sample surface [35]. The decane infiltration experiment shows that non radiative decay rates not taken into account in LDOS calculations may have an important contribution on lifetime. Other effects like local field electronic environment corrections have to be considered, as it is done in reference [34].

V. CONCLUSIONS

Opals prepared by sedimentation techniques and infiltrated by colloidal semiconductor nanocrystals have demonstrated a sufficient quality at a macroscopic scale to induce a modification of the nanocrystal emission. Both the emission diagram and the lifetime are affected by the opal. Due to the crystalline structure, the variation of the intensity with the collec-

tion angle is large and its dependence with the band structure has been modeled. Lifetime modification has been calculated with a computation of the local density of states, and the results are in good agreement with the measured around 4% decay time increase. When infiltrated with decane, we showed that the experimental variation cannot be explained just by the opal photonic bandgap and the local-field electronic environment effects on the dipole should not be neglected in the models.

A significant influence of the photonic bandgap on the lifetime would require a larger index contrast, or an inverse opal for which complete photonic bandgap can be achieved. The insertion of a defect [36, 37] inside opals, inducing a large modification of the LDOS, is a promising alternative to monitor the lifetime of nanocrystals embedded in 3D photonic crystals.

Acknowledgments

The authors gratefully acknowledge Karel Kunc for helpfull discussions and Emmanuelle Lacaze for AFM measurements. This study was supported by the Russian Foundation for Basic Research (projects N 07-02-90000 and N 07-02-92176) and C'Nano Ile de France.

[1] S. Laurent, S. Varoutsis, L. Le Gratiet, A. Lemaitre, I. Sagnes, F. Raineri, A. Levenson, I. Robert-Philip, and I. Abram, Applied Physics Letters 87 (2005).

[2] O. Gauthier-Lafaye, D. Mulin, S. Bonnefont, X. Checoury, J. Lourtioz, A. Talneau, and F. Lozes-Dupuy, IEEE Photonics Technology Letters 17, 1587 (2005).

[3] G. Ruani, C. Ancora, F. Corticelli, C. Dionigi, and C. Rossi, Solar Energy Materials and Solar Cells 92, 537 (2008).

[4] T. D. Happ, I. I. Tartakovskii, V. D. Kulakovskii, J.-P. Reithmaier, M. Kamp, and A. Forchel, Phys. Rev. B 66, 041303 (2002).

[5] W.-H. Chang, W.-Y. Chen, H.-S. Chang, T.-P. Hsieh, J.-I. Chyi, and T.-M. Hsu, Physical Review Letters 96, 117401 (2006).

[6] K. Hennessy, A. Badolato, M. Winger, D. Gerace, M. Atatuere, S. Gulde, S. Faelt, E. L. Hu, and A. Imamoglu, Nature 445, 896 (2007).

[7] T. Yoshie, A. Scherer, J. Hendrickson, G. Khitrova, H. Gibbs, G. Rupper, C. Ell, O. Shchekin, and D. Deppe, Nature 432, 200 (2004).

[8] N. Ganesh, W. Zhang, P. C. Mathias, E. Chow, J. A. N. T. Soares, V. Malyarchuk, A. D. Smith, and B. T. Cunningham, Nature Nanotechnology 2, 515 (2007).

[9] V. Reboud, N. Kehagias, M. Zelsmann, M. Striccoli, M. Tamborra, M. Curri, A. Agostiano, D. Mecerreyes, J. Alduncin, and C. Sotomayor Torres, Microelectronic Engineering 84, 1574 (2007).

[10] S. G. Romanov, M. Bardosova, D. E. Whitehead, I. M. Povey, M. Pemble, and C. M. S. Torres, Applied Physics Letters 90, 133101 (2007).

[11] E. Yablonovitch, Phys. Rev. Lett. 58, 2059 (1987).

[12] Z.-Y. Li and Z.-Q. Zhang, Phys. Rev. B 63, 125106 (2001).

[13] V. Solovyev, Journal of Applied Physics 94, 1205 (2003).

[14] M. Megens, J. E. G. J. Wijnhoven, A. Lagendijk, and W. L. Vos, Phys. Rev. A 59, 4727 (1999).

[15] I. S. Nikolaev, P. Lodahl, A. F. van Driel, A. F. Koenderink, and W. L. Vos, Phys. Rev. B 75, 115302 (2007).

[16] P. Lodahl, A. F. van Driel, I. S. Nikolaev, A. Irman, O. Karin, D. Vanmaekelbergh, and W.

L. Vos, Letters to Nature 430, 654 (2004).

[17] M. Barth, R. Schuster, A. Gruber, and F. Cichos, Physical Review Letters 96, 243902 (2006).

[18] A. Blanco, C. Lopez, R. Mayoral, H. Miguez, F. Meseguer, A. Mifsud, and J. Herrero, Applied Physics Letters 73, 1781 (1998).

[19] Y. A. a. Valsov, Applied Physics Letters 71, 1616 (1997).

[20] Y. Lin, J. Zhang, E. H. Sargent, and E. Kumacheva, Applied Physics Letters 81, 3134 (2002).

[21] C. M. Chuang, W. B. Lu, W. F. Su, C. M. Lin, and Y. F. Chen, Journal of Applied Physics 97, 096104 (2005).

[22] K. Liu, T. Schmedake, K. Daneshvar, and R. Tsu, Microelectronics Journal 38, 700 (2007).

[23] S. Gaponenko, Journal of Luminescence 87-89, 152 (2000).

[24] S. G. Romanov, T. Maka, C. M. S. Torres, M. Müller, and R. Zentel, Journal of Applied Physics 91, 9426 (2002).

[25] R. A. L. Vallée, K. Baert, B. Kolaric, M. V. der Auweraer, and K. Clays, Phys. Rev. B 76, 045113 (2007).

[26] M. Barth, A. Gruber, and F. Cichos, Phys. Rev. B 72, 085129 (2005).

[27] M. Romanelli, C. Vion, C. Barthou, P. Benalloul, J. Frigerio, and A. Maitre, Journal of the Korean Physical Society 52, 1589 (2008).

[28] A. N. Gruzintsev, G. A. Emel'chenko, V. M. Masalov, M. Romanelli, C. Barthou, P. Benalloul, and A. Maitre, Inorganic Materials 44, 159 (2008).

[29] S. G. Johnson and J. D. Joannopoulos, Opt. Express 8, 173 (2001).

[30] Y. Xia, B. Gates, and S. Park, Journal of Lightwave Technology 17, 1956 (1999).

[31] A.F. van Driel, I.S. Nikolaev, P. Vergeer, P. Lodahl, D. Vanmaekelbergh, and W.L. Vos, Phys. Rev. B 75, 035329 (2007).

[32] S. G. Romanov, T. Maka, C. M. Sotomayor Torres, M. Müller, R. Zentel, D. Cassagne, J. Manzanares-Martinez, and C. Jouanin, Phys. Rev. E 63, 056603 (2001).

[33] X. Gonze, J. M. Beuken, R. Caracas, F. Detraux, M. Fuchs, G. M. Rignanese, L. Sindic, M. Verstraete, G. Zerah, F. Jollet, et al., Computational Materials Science 25, 478 (2002).

[34] S. F. Wuister, C. de Mello Donega and A. Meijerink, J. Chem. Phys. 121, 4310 (2004)

[35] G. Schlegel, J. Bohnenberger, I. Potapova and A. Mews, Phys. Rev. Lett. 88, 137401 (2002) ; B. R. Fisher, H.-J. Eisler, N. E. Stott and M. G. Bawendi, J. Phys. Chem. B 108, 143 (2004).

[36] P. Massée, S. Reculusa, K. Clays, and S. Ravaine, Chemical Physics Letters 422, 251 (2006).

[37] E. Palacios-Lidon, J. Galisteo-Lopez, B. Juarez, and C. Lopez, Advanced Materials 16, 341 (2004).

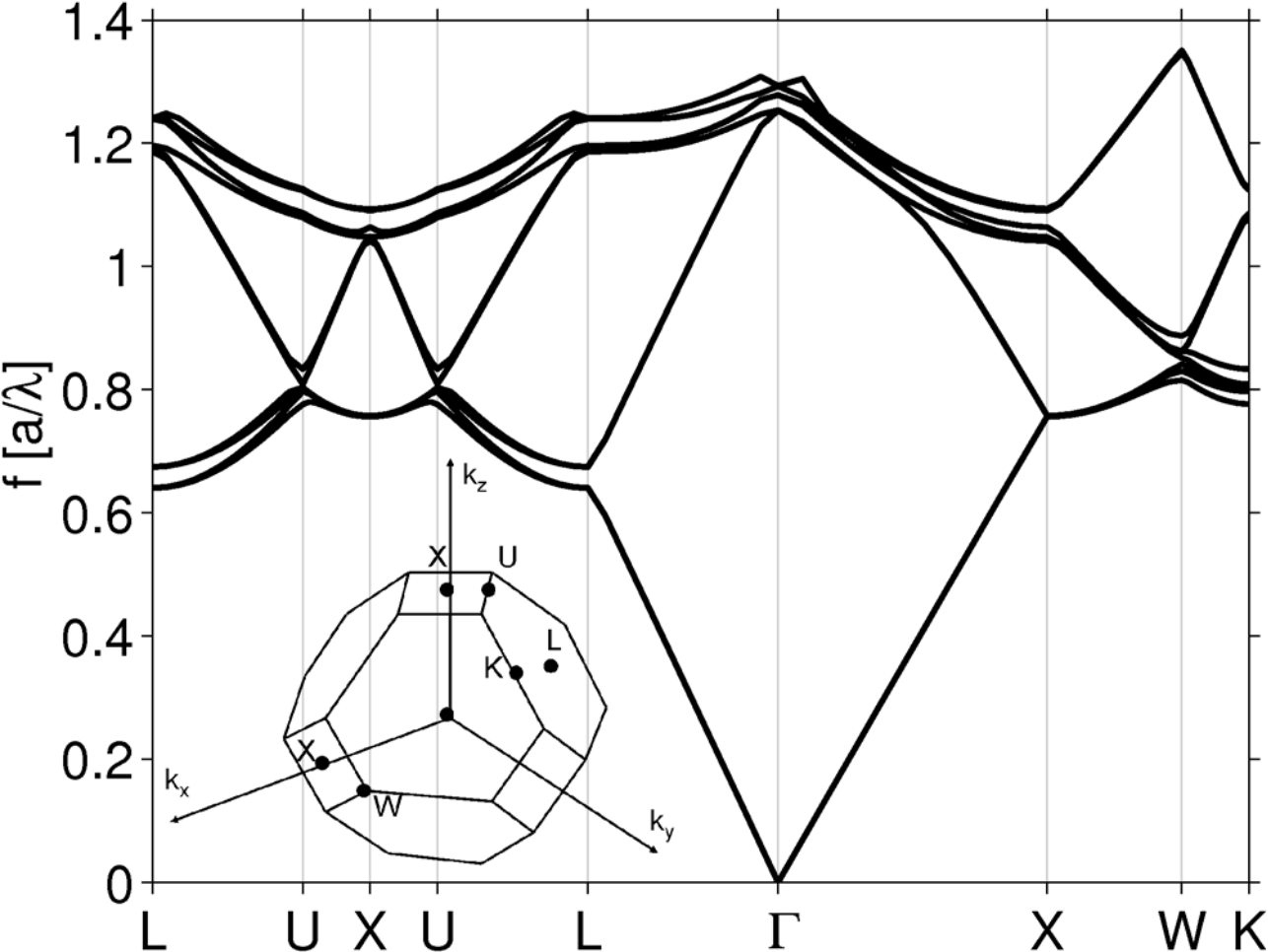
1.4
1.2
1
0.8
0.6
0.4
0.2
0
f [a/λ]
L
U
X
U
L
Γ
X
W
K
k_z
X
U
L
K
X
W
k_x
k_y

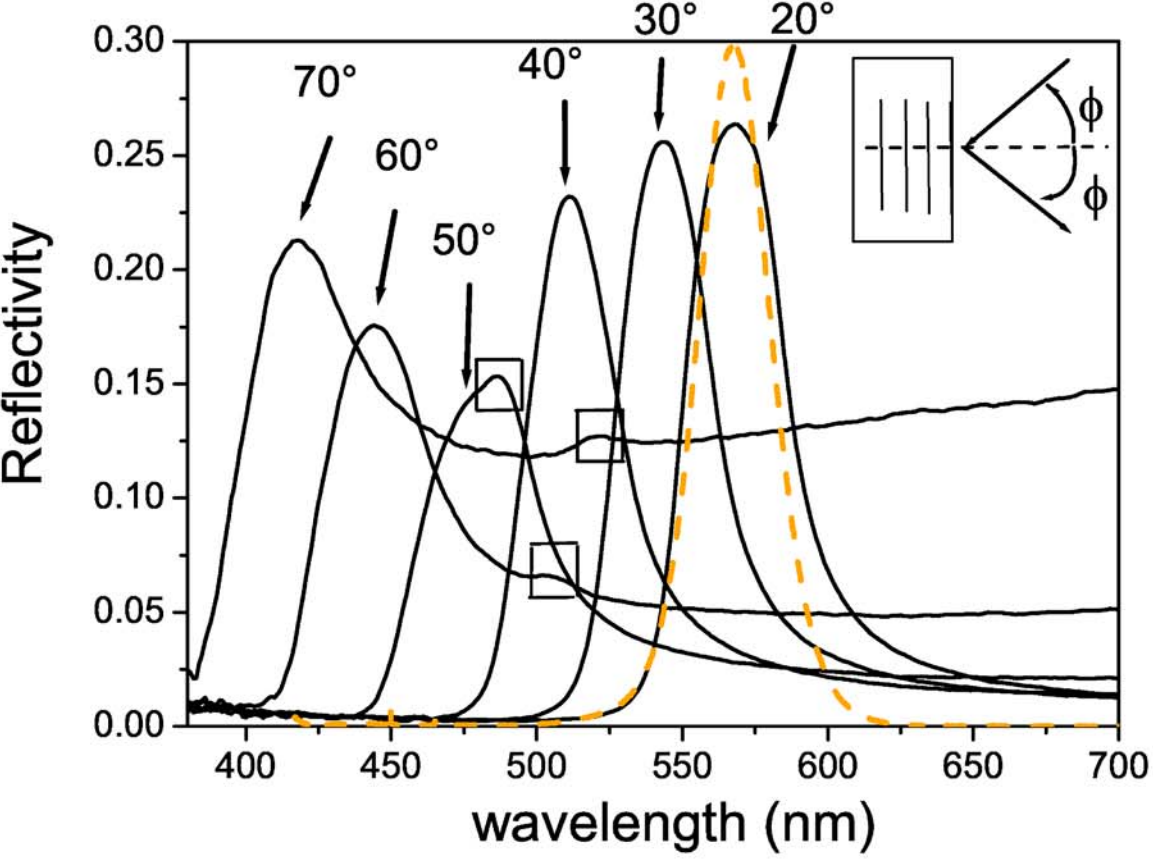
Reflectivity
wavelength (nm)
70°
60°
50°
40°
30°
20°
ϕ
ϕ

(a)

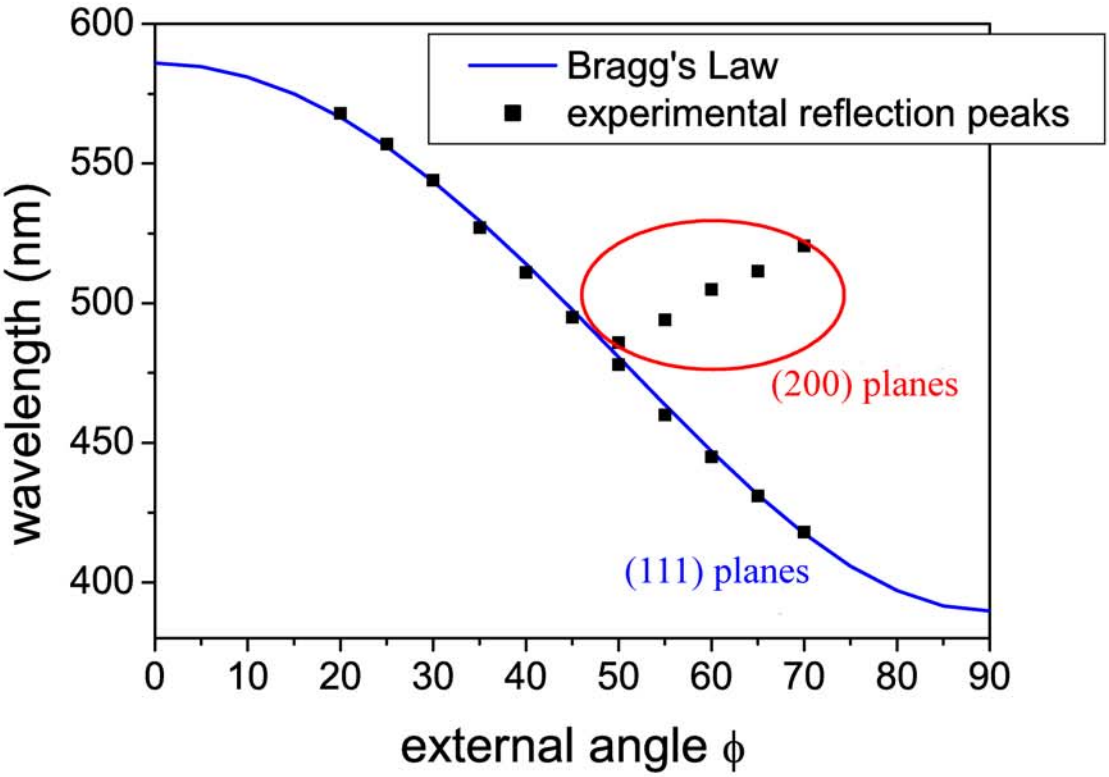
Bragg's Law
experimental reflection peaks
(200) planes
(111) planes
wavelength (nm)
external angle ϕ

(b)

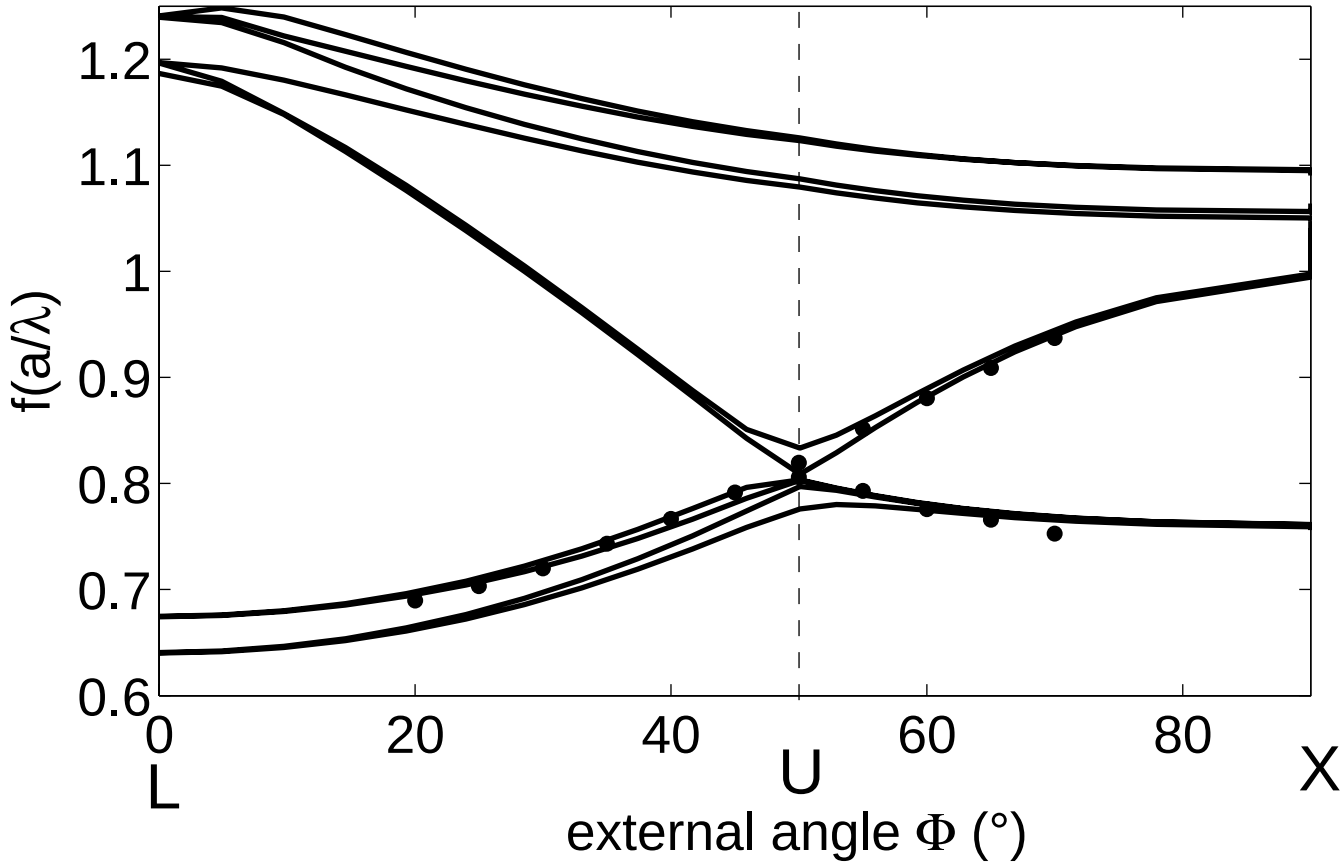
1.2
1.1
1
0.9
0.8
0.7
0.6
f(a/λ)
0
20
40
60
80
L
U
X
external angle Φ (°)

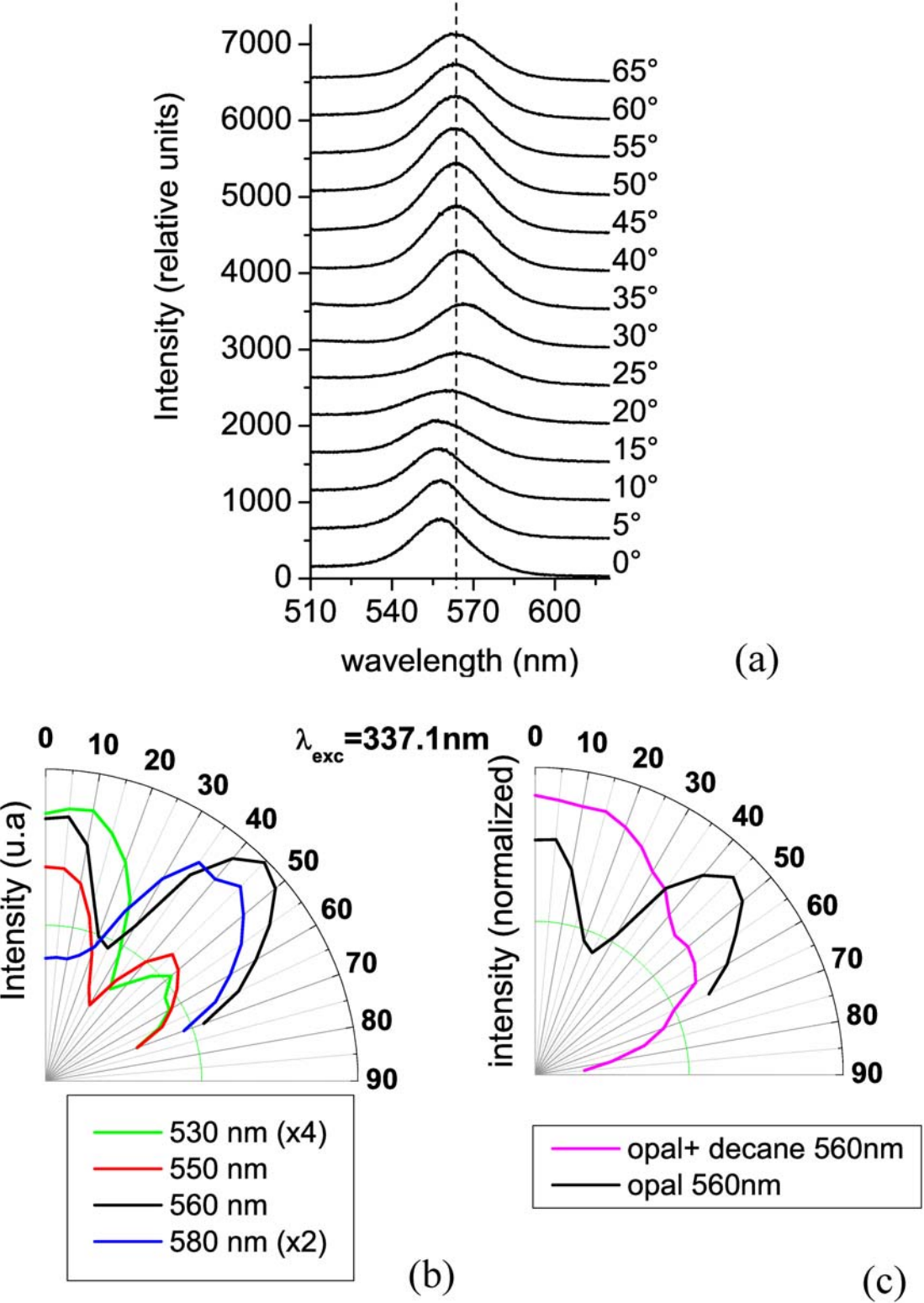
Intensity (relative units)
7000
6000
5000
4000
3000
2000
1000
0
65°
60°
55°
50°
45°
40°
35°
30°
25°
20°
15°
10°
5°
0°
510
540
570
600
wavelength (nm)
(a)
λexc=337.1nm
0
10
20
30
40
50
60
70
80
90
Intensity (u.a)
530 nm (x4)
550 nm
560 nm
580 nm (x2)
(b)
intensity (normalized)
opal+ decane 560nm
opal 560nm
(c)

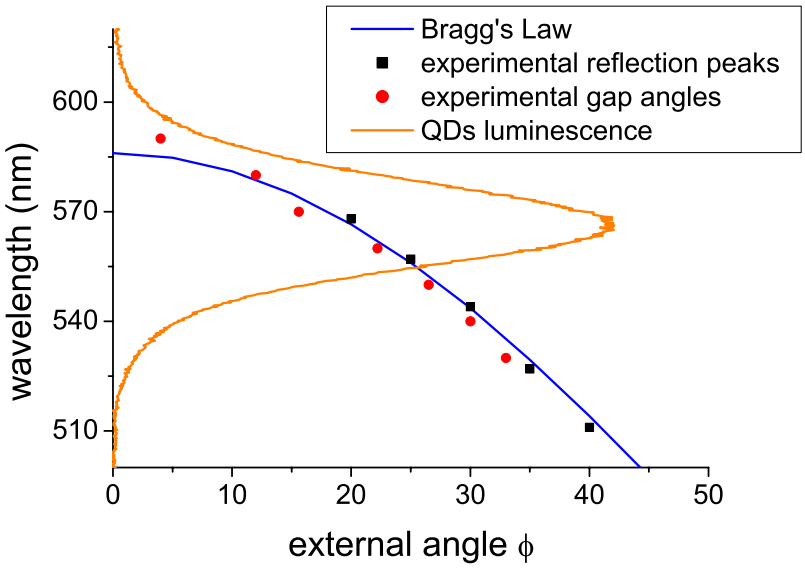
Bragg's Law
experimental reflection peaks
experimental gap angles
QDs luminescence
wavelength (nm)
600
570
540
510
0
10
20
30
40
50
external angle ϕ

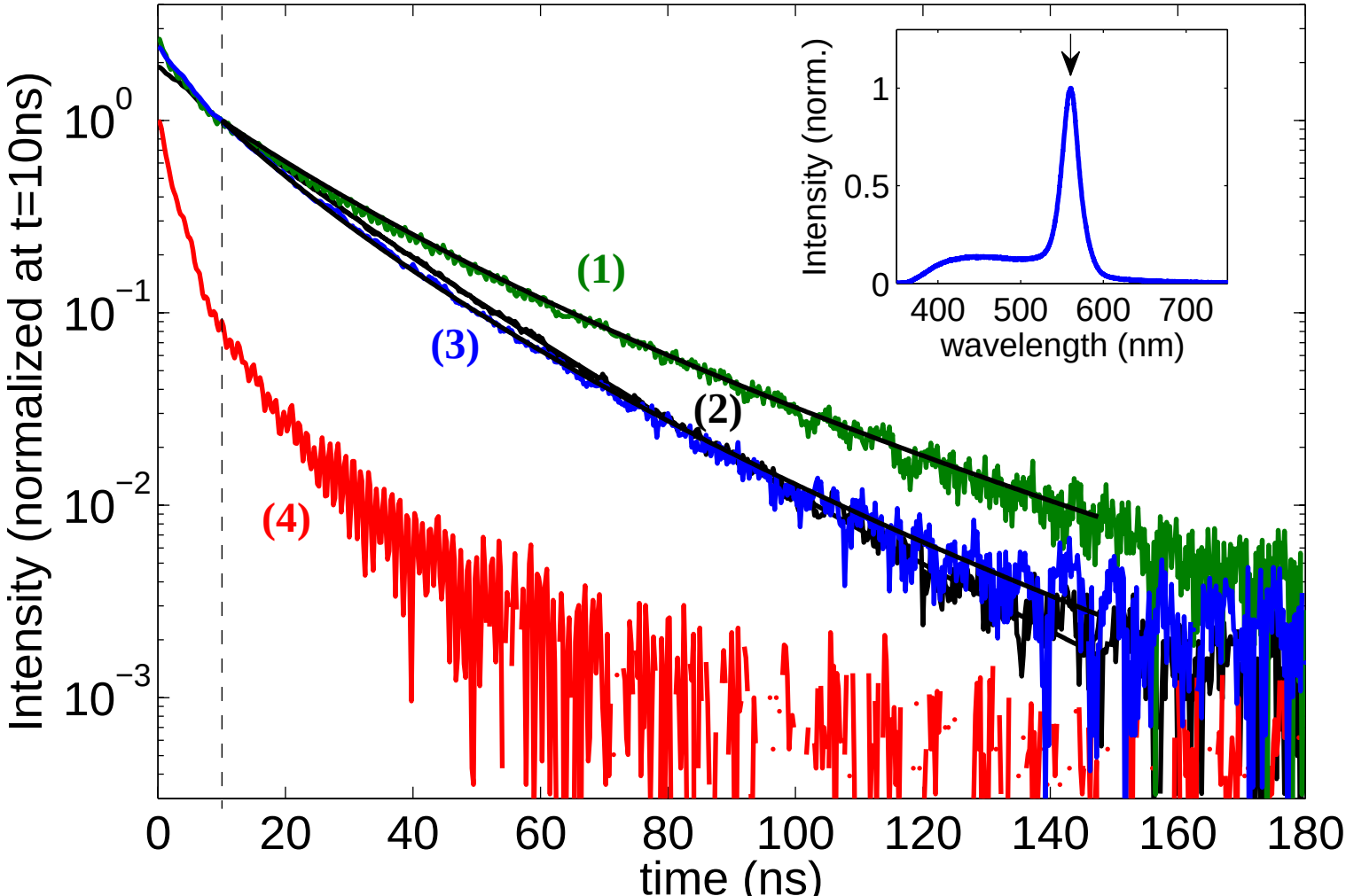
Intensity (normalized at t=10ns)
10^{0}
10^{-1}
10^{-2}
10^{-3}
0
20
40
60
80
100
120
140
160
180
time (ns)
(1)
(2)
(3)
(4)
Intensity (norm.)
1
0.5
0
400
500
600
700
wavelength (nm)

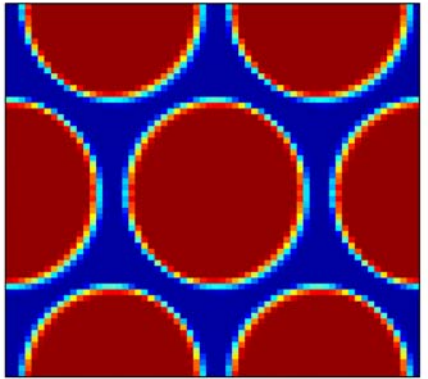

(a)

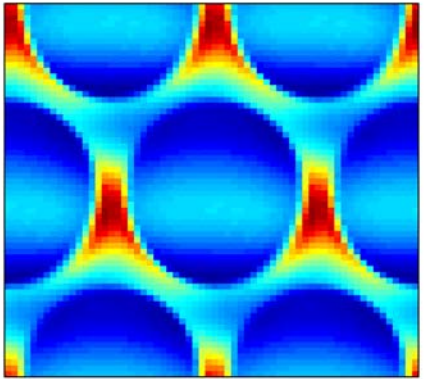

(b)

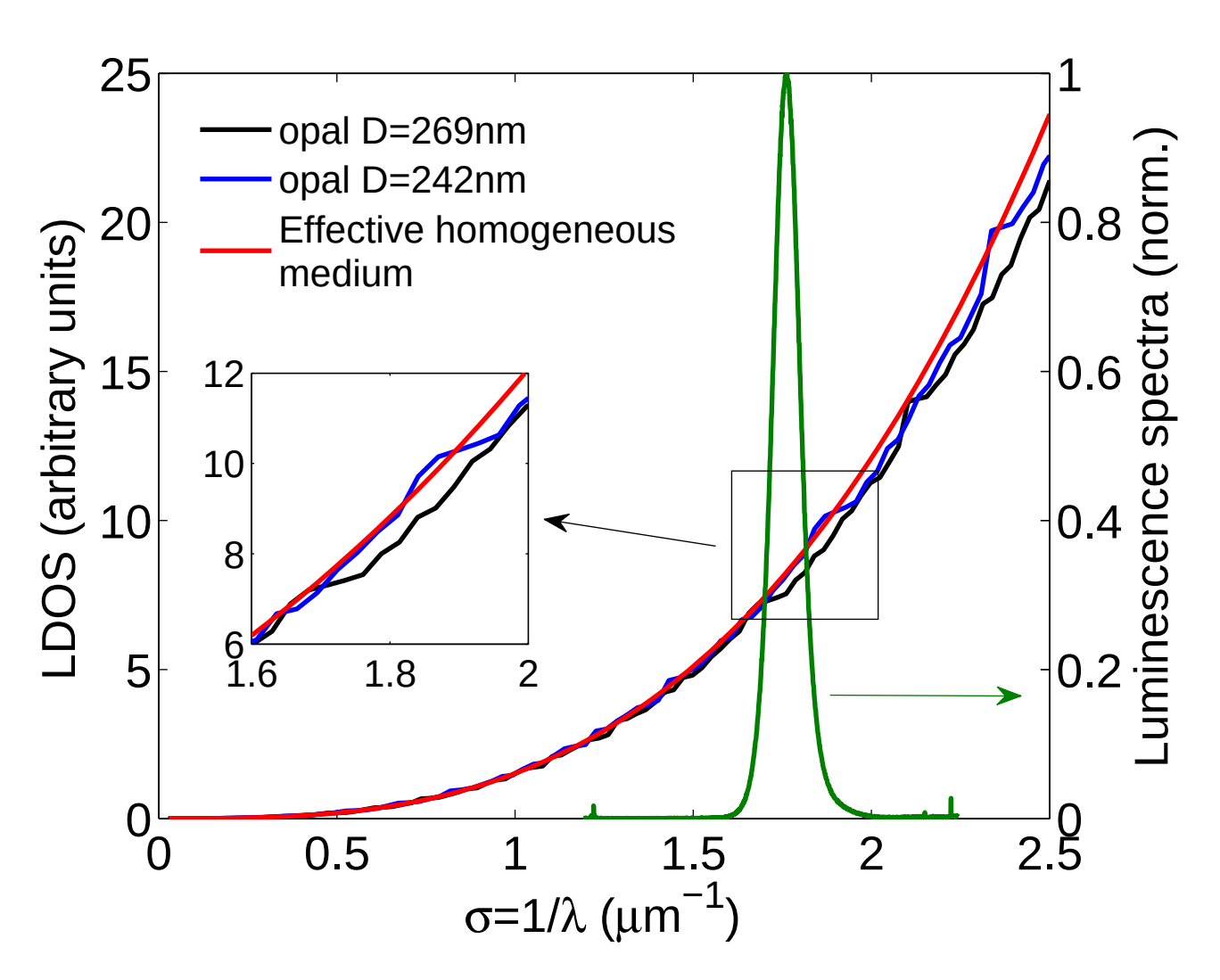
opal D=269nm
opal D=242nm
Effective homogeneous medium
LDOS (arbitrary units)
Luminescence spectra (norm.)
σ=1/λ (μm^{-1})
0
5
10
15
20
25
0.2
0.4
0.6
0.8
1
0.5
1.5
2
2.5
6
8
10
12
1.6
1.8